Sixth International Symposium on Marine Propulsors
smp'19, Rome, Italy, May 2019

On the development and verification of diffused endplate propeller

Young-Zehr Kehr[1], Huan-Jia Xu[1,2], Jui-Hsiang Kao[1]

[1]Department of Systems Engineering and Naval Architecture, National Taiwan Ocean University (NTOU), Keelung, Taiwan, R.O.C
[2]Research engineer, Hung Shen Propeller Company, LTD, Pingtung, Taiwan, R.O.C

ABSTRACT

In this paper, a tip endplate propeller with innovative conception is proposed, and its performance verified by experiments is presented. The proposed propeller, ENDP, is shaped by a diffused endplate which is bent to the pressure side. According to the experiments conducted in the cavitation tunnel, the ENDP can not only restrain the tip vortex cavitation but also eliminate the sheet cavitation that can typically be found on the outer surface of the endplate of the CLT propeller, especially when propeller is operating at inclined shaft condition. Moreover, the thrust of the ENDP propeller is mainly contributed by the propeller pressure side, the cavitation on the back of the propeller is remarkably reduced; thus, the expand area ratio of the ENDP can be reduced to attain higher efficiency. Besides, the ENDP propeller can also reduce the possibility of thrust breakdown; thus, the ENDP propeller is more suitable for the accelerating condition (i.e. the heavy-load condition).

Keywords

Diffused endplate propeller, Cavitation control, Tip vortex cavitation, Sheet cavitation

1 INTRODUCTION

For marine propellers, efficiency and cavitation are both important issues. As cavitation appears, noise, vibration, and thrust breakdown will all be induced. In general, propeller efficiency is to be reduced to control the cavity volume on its surface. In order to control the cavitation without efficiency loss, the tip fin propeller was proposed.

The tip fin propeller can be classified into tip endplate propeller and tip raked propeller. Firstly, the tip endplate propeller, so called tip vortex free propeller (TVF) was developed by Gómez (1976), in which the tip endplate was bend to pressure side, and located tangentially to a cylinder coaxial with the shaft line. Since the stream surface passing through the propeller disk suffers a noticeable contraction, it was decided to locate the endplate tangentially to the stream surface. This type of propeller is called contracted loaded tip propeller (CLT propeller) by Gómez and Adalid (1992,1998). Due to the contraction of the endplate, the propeller radius at the trailing edge is lower than that at leading edge for a CLT propeller. According to the New Momentum Theory derived by Gómez and Adalid (1992), it was proved that the thrust of CLT propeller is much more contributed by the pressure side. Thus, the low pressure on the suction side of the propeller can be reduced. Consequently, the CLT propeller can control the cavitation on suction side much better than conventional propellers. Besides, because the tip is loaded, the effective diameter of the CLT propeller is larger than that of the conventional propeller. Thus, the CLT propeller is more suitable for the ship with small stern space where only propeller with small optimal diameter can be installed.

Sánchez-Caja et al. (2006) used k-ε turbulent model to simulate the performance of CLT propellers and illustrated that an inverse flow appears on the leading edges of the blade outer region and tip plate. The sheet cavitation was caused due to the inverse flow. The statements mentioned by Sánchez-Caja et al. (2006) were also proved by Kehr and Wu (2010), and Bertetta et al. (2012). Though the CLT propeller can restrain the tip vortex cavitation effectively, the serious sheet cavitation on the outer surface of the tip endplate is generated, especially when propeller operating at inclined shaft condition, as shown by Kehr and Wu (2010). Sánchez-Caja et al. (2012) modified the tip plate of the CLT propellers by different contracted angles, swept angles, flap angles, and depth of plate cutting, the results indicated that the efficiency can be increased by decreasing the contracted angle and flap angle. In addition, backward swept and high-depth cutting of the plate are not suggested for attaining higher thrust. Tip unloading was applied by Gaggero et al. (2016), and resulted in 10~20% reduction of the cavity volume. However, the sheet cavitation on the outer surface of the endplate still appeared, and will cause the unexpected vibration and noise.

The aim of this paper is to eliminate the back sheet cavitation on the outer surface of the endplate. The proposed innovative propeller is designed with diffused endplate, and named as ENDP. The results observed in

* Corresponding Author, Huan-Jia Xu:10351028@email.ntou.edu.tw

the cavitation tunnel show that the ENDP propellers can eliminate the cavitation appearing on the outer surface of the endplate, especially when propeller is operating at inclined shaft condition. Besides, the experiments were conducted for comparing an ENDP propeller with a conventional one. These two propellers were designed at the same operating condition. The results show that the ENDP propeller is superior to the conventional one. The efficiency of ENDP propeller is higher than that of conventional propeller at the design point. Moreover, the ENDP propeller can keep higher efficiency at the heavy-load condition; thus, the ENDP propeller is more suitable for accelerating condition.

2 Cavitation investigation of CLT propellers

According to Blade Momentum Theory, the inflow of the operating propeller will be accelerated and contracted due to the suction effect. Thus, the tip endplate was shaped as contracted type for preventing the inflow from being obstructed by the tip endplate.

However, Kehr & Wu (2010) conducted series tests of CLT propellers in the cavitation tunnel of National Taiwan Ocean University(NTOU), and it is shown that a serious sheet cavitation appeared starting from the leading edge of the endplate. In Figure 1, the contracted angle of the endplate for the CLT propeller is 1.0°, and a serious sheet cavitation appears from the leading edge of the endplate. Kehr & Wu (2010) reduced the contracted angle of tip endplate from 1.0° to 0.1° in order to eliminate the back sheet cavitation on the outer surface of endplate. However, Figure 2 shows that the back sheet cavitation on the outer surface of endplate is still generated when propeller operating at same cavitation number and propeller thrust loading. It should be noticed that though the contracted angle is only 0.1 °,the attack angle at the endplate is still large enough to cause the back sheet cavitation on the outer surface of endplate. This shows that the inflow itself forms a positive attack angle to the endplate. In other words, the thoughts in 1990s that the endplate of the propeller should be contracted should be modified for the tip loaded propeller.

Figure 1. The back sheet cavitation on the outer suface of endplate with 1.0° contracted angle, Ae/Ao=0.55, P/D=0.965 at n=29.41RPS,σ=1.50,J=0.70,K_T/J^2=0.390,0°inclined shaft condition.($Rn_{0.7r} = 8.1\times10^5$)

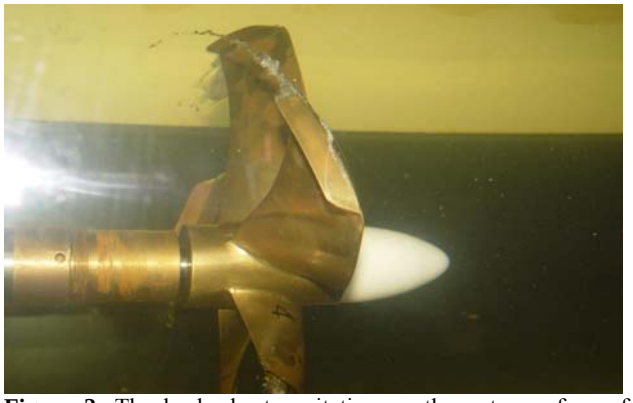

Figure 2. The back sheet cavitation on the outer surface of endplate with 0.1° contracted angle, A_e/A_o=0.55, P/D=0.991 at n=26.67RPS,σ=1.50,J=0.75,K_T/J^2=0.393,0°inclinedshaft condition.($Rn_{0.7r} = 7.5\times10^5$)

3 The innovation of ENDP propellers

The tip endplate of the tip loaded propeller can prevent the tip vortex on the pressure side from moving to the suction side. Thus, remarkable high pressure still exists on the face near the blade tip. The high pressure on the face near the tip endplate will obstruct the inflow flowing into the blade, and force the inflow flowing toward outside of the endplate as illustrated in Figure 3. Therefore, the tip loaded propeller should be shaped as diffused type for reducing the large attack angle which will result in sheet cavitation on the outer surface of endplate.

Figure 4 indicates the definition of the diffused and contracted angles at the tip endplate. The black line is the cylindrical surface, the blue dotted line is the contracted endplate, and the red dotted line is the diffused endplate.

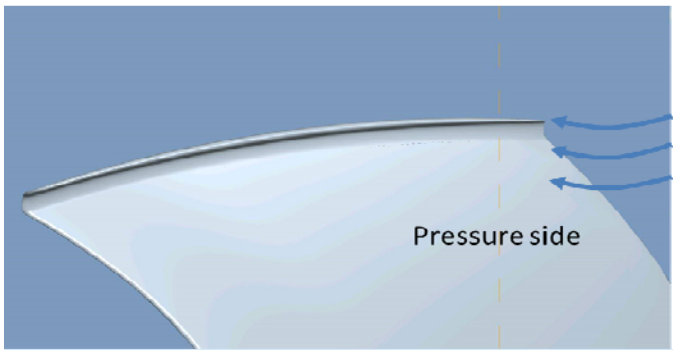

Figure 3. The inflow at the leading edge of the tip endplate.

The experiments are carried out in the medium-sized cavitation tunnel K12 of National Taiwan Ocean University. The test section of the cavitation tunnel is 0.5m height and 0.5m wide, and the maximal inflow speed in the test section is about 11.6 m/s. A tiltable dynamometer, H39-27, manufactured by Kempf & Remmers is installed. Not only the thrust and torque generated by the propeller, but also the vertical and horizontal forces due to the inclined shaft angle can be measured by the dynamometer. Thus, it is allowable to test the propeller operating with inclined shaft angles. Besides, a mobile stroboscopic system is used to visualize the cavitation phenomena.

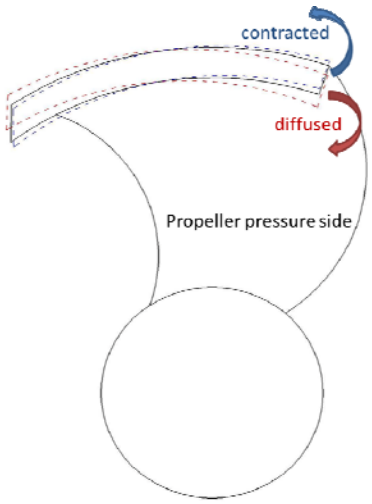

Figure 4. The definition of the contracted and diffused tip endplates

In this paper, four model propellers with diffused tip endplates and a conventional propeller are tested. The main parameters for the model propellers are listed in Table 1. P1 is designed for a large OPV. Its inclined shaft angle is only 3°. It can represent the characteristics of horizontal shaft. P2, P3 and P4 have a similar propeller thrust loading, and operating for high-speed craft at inclined shaft between 8° and 10°. Their open-water diagrams are shown in Figure 5. P2 is designed with trailing edge cup and with a small diffused angle of endplate in order to demonstrate the influence of the inclined shaft angle on the back sheet cavitation of the endplate. P3 and P4 are designed with a 1.0° diffused angle of endplate, however, with different Ae/Ao.

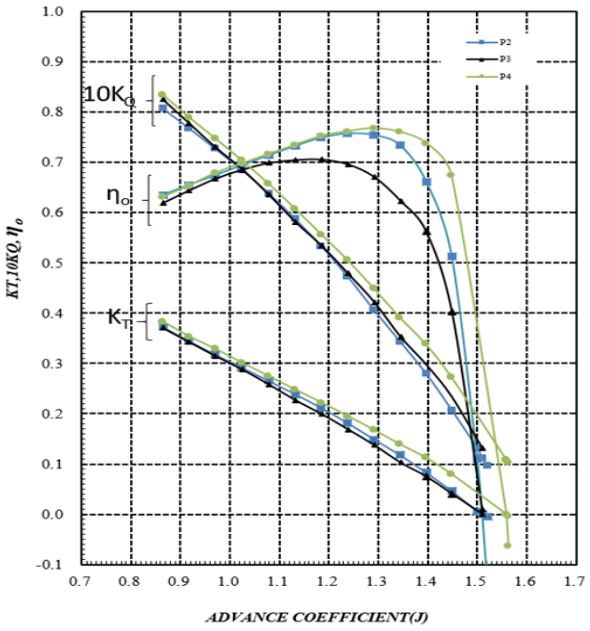

Figure 5. The propeller open-water diagram of P2,P3 and P4 at ATM and 0° inclined shaft condition.

The cavitation number, σ, is defined by Equation (1). The cavitation index is based on the height of shaft axis.

$$\sigma = \frac{P_0 + \rho g h - P_v}{\frac{1}{2}\rho v^2} \text{ or } \frac{P_t - P_v}{\frac{1}{2}\rho v_t^2} \qquad (1)$$

Where P_0 =atmospheric pressure, v =the inflow velocity, P_v =the vapor pressure, ρ = the density of fluid, g=the gravity acceleration, and h=the shaft immersion. P_t =tunnel pressure, and v_t =the tested speed at tunnel.

Reynolds number($Rn_{0.7r}$) shown in this paper is defined by Equation (2), and it is based on 0.7 radial position of propeller.

$$Rn_{0.7r} = \frac{UC_{0.7r}}{\upsilon} \qquad (2)$$

Where U=the resultant velocity of 0.7 radial position of propeller, $C_{0.7r}$=the chord length of propeller at 0.7 radial position, and υ =kinematic viscosity of seawater at 15.6°C, 1.17×10^{-6} (m^2/s)

Table 1. The main dimensions for the model ENDP propellers

Model propeller	P1	P2	P3	P4	P5
Propeller type	ENDP	ENDP	ENDP	ENDP	Conventional
Diameter(mm)	220.5	250.0	250.0	250.0	250.0
Hub ratio	0.27	0.20	0.20	0.20	0.20
Pitch-Dia.-ratio	1.1230	1.2708	1.4100	1.3988	1.4100
Blade area ratio	0.760	0.700	0.921	0.800	1.000
No. of blades	5	4	4	4	4
Diffused angle(deg)	0.3	0.3	1.0	1.0	

3.1 Operating at horizontal shaft condition

In Figure 6, the innovative propeller P1 including 0.3° diffused angle at the endplate is proposed for operating at zero inclined shaft angle condition, and σ= 1.5, K_T/J^2=0.393. Figure 6 shows that the diffused endplate propeller can eliminate the back sheet cavitation on the outer surface of the endplate. Therefore, the diffused angle of the endplate is recommended to be 0.3° for 0° inclined shaft angle condition, when the propeller operates at K_T/J^2=0.393. The stronger propeller loading will cause the back sheet cavitation on the outer surface of the endplate more easily. Thus, the optimal diffused angle of endplate should be increased accordingly as the propeller thrust loading is increased. It can be determined by CFD calculation. Cp contours shown in Figures 7 and 8 are computed by the CFD according to different propeller thrust loadings respectively. The propeller thrust loading of Figure 8 is higher than that of Figure 7 by 40%. Consequently, low-pressure region of Figure 8 is larger than that of Figure 7, and the sheet cavitation may appear in the low-pressure region.

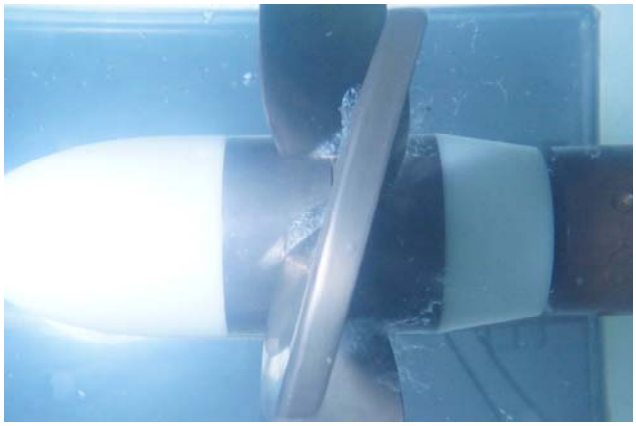

Figure 6. The experimental result of P1(0.3º diffused angle) at n=29.42 RPS, σ=1.50, J=0.7706, K_T/J^2=0.393, 0º inclined shaft condition ($Rn_{0.7r} = 1.0 \times 10^6$)

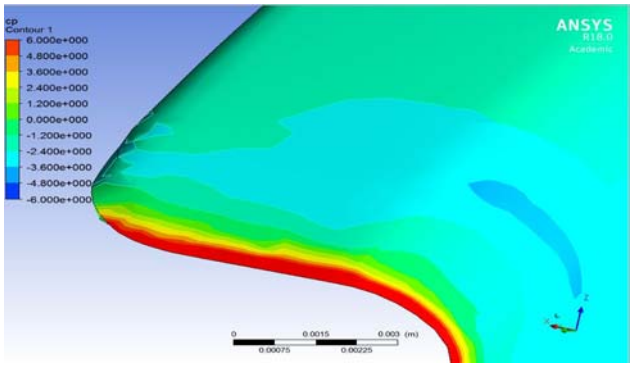

Figure 7. The Cp contour of endplate propeller with 0.0º diffused angle at K_T/J^2=0.393, 0º inclined shaft condition

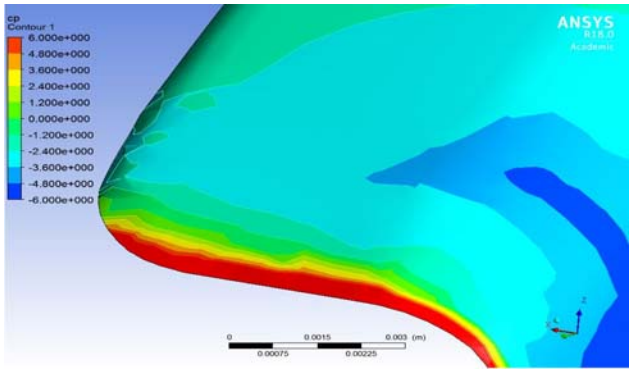

Figure 8. The Cp contour of endplate propeller with 0.0º diffused angle at K_T/J^2=0.550, 0º inclined shaft condition

3.2 Operating at inclined shaft condition

In Figure 9, V_1 is the inflow along the hull bottom and it is equal to the inflow velocity, V, mentioned in Equation(3). Besides, V_o is the axial velocity component for the propeller and it is equal to $V_1 \cos \psi$ .If a propeller operates with inclined shaft angle, extra velocity perpendicular to the shaft will be induced. Figure 9 indicates that a vertical velocity relative to the shaft, $V_1 \sin \psi$, will be induced by the inclined shaft angle, ψ . Figure 10 shows the resultant inflow for the tip endplate, VR, at different blade angles. ωr is the tangential inflow speed due to the propeller rotating. Figure 10 illustrates that the increment of the attack angle for the tip endplate at 0º position (i.e. twelve-o'clock position) is the largest due to the vertical velocity, $V_1 \sin \psi$. The additional increment of attack angle at endplate due to inclined shaft will cause serious back sheet cavitation on the outer surface of endplate.

On the other hand, when propeller blade turns to the 180º circumferential position, the cylindrical tangential inflow velocity ωr with $V_1 \sin \psi$ will form a negative angle for the endplate. This negative attack angle combined with diffused angle of endplate will result in a larger negative attack angle, which will generate a low pressure zone at the inner side of the leading edge of the tip endplate. However, the low pressure zone is adjacent to the high pressure on the face side of the propeller, and the immerged depth of the endplate at this position is deeper. Therefore, cavitation is not easy to occur. Hence, it is important to determine a suitable diffused angle which will not cause cavitation on endplate both at 0º and 180º circumferential positions.

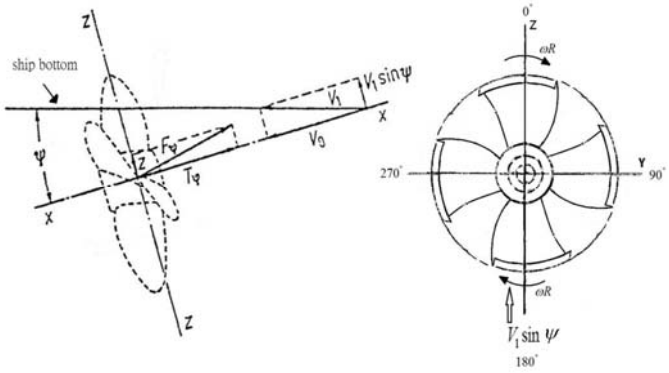

Figure 9. The inflow velocities with inclined shaft angle

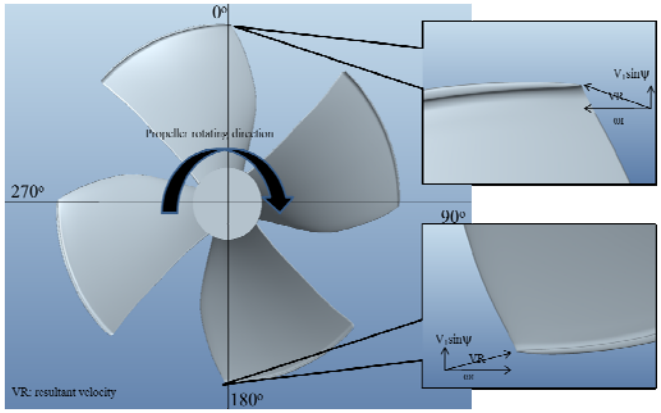

Figure 10. The attack angle for the tip endplate at different blade angles with inclined shaft angle

In Figures 11, 12, 13, and 14, the back cavitation on the outer surface of endplate of the P2 propeller for different inclined shaft angles (8º, and 10º) and cavitation numbers are shown at 0º circumferential position. The advance ratio, J, for Figures 11, 12, 13, and 14 is 1.12. The advance ratio, J, is defined by Equation(3):

$$J = \frac{V}{nD} \qquad (3)$$

Where V =the inflow velocity of the propeller, n=the shaft rotating speed, and D=the propeller diameter.

The attack angle of the tip endplate will be increased due to the vertical velocity which is induced by the inclined shaft angle. In Figure 11, 12, 13, and 14, it can be

observed that the back sheet cavitation on the outer surface of endplate appears from the leading edge of the tip endplate, and the cavitation extension gradually increases as the cavitation number decreases. In Figure 11, the back sheet cavitation on the outer surface of endplate appears for both 8° and 10° inclined shaft angles. The extension and the thickness of the back sheet cavitation on the outer surface of endplate are greater as the propeller operates with 10° inclined shaft angle. It is reasonable because the attack angle at the tip endplate will be larger for 10° inclined shaft angle. The comparisons in Figure 12 and Figure 13 are similar to that in Figure 11. Because the cavitation number is the lowest in Figure 14 (i.e. σ=0.50), it can be observed that the back sheet cavitation extension on the outer surface of endplate exceeds the whole tip endplate. The back sheet cavitation on the outer surface of endplate will cause the unexpected noise and vibration.

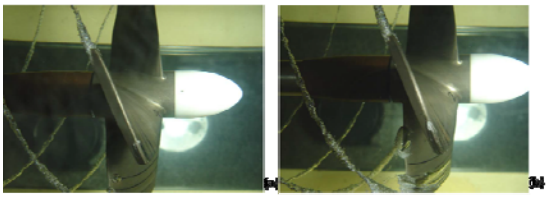

Figure 11. The experimental results of P2 at (a) 8° inclined shaft, K_T/J^2=0.236 and (b) 10° inclined shaft, K_T/J^2=0.232 at n=25.00 RPS, σ=1.00 when blade turning to 0° circumferential position ($Rn_{0.7r} = 1.2 \times 10^6$)

Figure 12. The experimental results of P2 at (a) 8° inclined shaft, K_T/J^2=0.210 and (b) 10° inclined shaft, K_T/J^2=0.201 at n=25.00 RPS, σ=0.75 when blade turning to 0° circumferential position ($Rn_{0.7r} = 1.2 \times 10^6$)

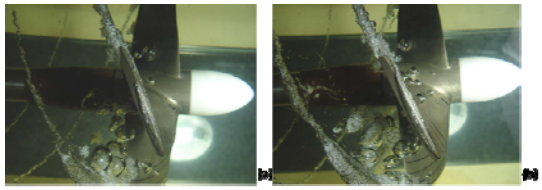

Figure 13. The experimental results of P2 at (a) 8° inclined shaft, K_T/J^2=0.187 and (b) 10° inclined shaft, K_T/J^2=0.166 at n=25.00 RPS, σ=0.60 when blade turning to 0° circumferential position ($Rn_{0.7r} = 1.2 \times 10^6$)

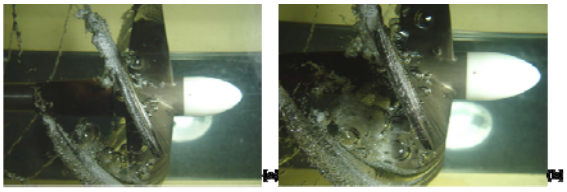

Figure 14. The experimental results of P2 at (a) 8° inclined shaft, K_T/J^2=0.146 and (b) 10° inclined shaft, K_T/J^2=0.120 at n=26.78 RPS, σ=0.50 when blade turning to 0° circumferential position ($Rn_{0.7r} = 1.3 \times 10^6$)

In Figures 15 ~ 17, the cavitation on the outer surface of endplate of the P3 propeller at 0° circumferential blade position for different cavitation numbers are shown respectively. The advance ratio, J, for Figures 15~17 is 1.08, and the corresponding propeller thrust loading is higher than that of P2. According to the experimental results, the back sheet cavitation on the outer surface of endplate disappeared at 0° circumferential blade position when cavitation number is down to 0.50 and inclined shaft angle is up to 10°.

Comparing with 14(b) and 17(b), P2 and P3 operate at the worst condition (i.e. the cavitation is the lowest, and the inclined shaft angle is the largest). It is found that the cavitation in Figure 14(b) disappears in Figure 17(b). Besides, the cavitation on inner side of endplate of P3 at σ=0.50, 10° inclined shaft condition can not be found at 180° circumferential position, as shown in Figure 18. Authors have also tested ENDP propeller with 1.2° diffused angle of the endplate, and have found the cavitation on the inner surface of endplate at 180° circumferential blade position when propeller operates at 10° inclined shaft condition, and at low cavitation number. P4 has a similar result as P3 about the control of back sheet cavitation on the endplate. That means Ae/Ao is not an important parameter when propeller operating at high inclined shaft condition. As the inclined shaft angle for high speed craft is normally between 8° to 11° dependent on the ship size and ship speed, 1.0° diffused angle for the tip endplate of the ENDP propeller is suggested for inclined shaft angle higher than 10°. If the inclined shaft angle is lower than 10° and the cavitation number is higher than 0.75, a 0.8° diffused angle for the endplate of the ENDP propeller can be considered.

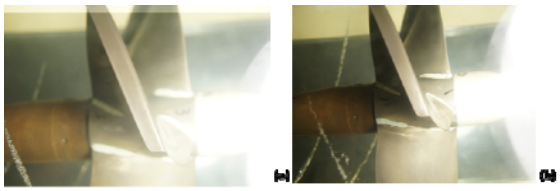

Figure 15. The experimental results of P3 at (a) 8° inclined shaft, K_T/J^2=0.260 and (b) 10° inclined shaft, K_T/J^2=0.256 at n=22.22 RPS, σ=1.00 when blade turning to 0° circumferential position ($Rn_{0.7r} = 1.4 \times 10^6$)

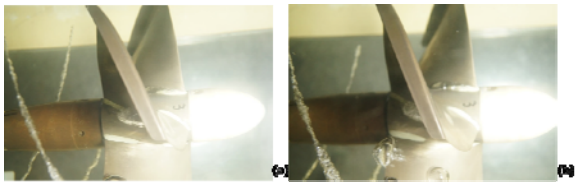

Figure 16. The experimental results of P3 at (a) 8° inclined shaft, K_T/J^2=0.246 and (b) 10° inclined shaft, K_T/J^2=0.240 at n=24.07 RPS, σ=0.75 when blade turning to 0° circumferential position ($Rn_{0.7r} = 1.5 \times 10^6$)

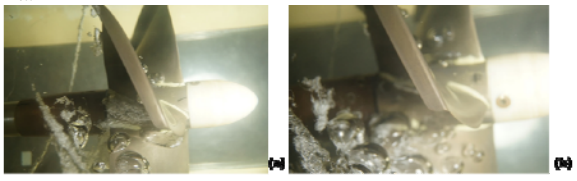

Figure 17. The experimental results of P3 (a) 8° inclined shaft,

K_T/J^2=0.187 and (b) 10° inclined shaft, K_T/J^2=0.170 at n=27.78 RPS, σ=0.50 when blade turning to 0°circumferential position ($Rn_{0.7r} = 1.7\times10^6$)

Figure 18. The experimental results of P3 (a) 8° inclined shaft, K_T/J^2=0.187 and (b) 10° inclined shaft, K_T/J^2=0.170 at n=27.78 RPS, σ=0.50 when blade turning to 180°circumferential position ($Rn_{0.7r} = 1.7\times10^6$)

3.3 Comparison between ENDP propeller and conventional propeller

Figure 19 illustrates the open-water diagram of P4 propeller and a conventional propeller P5. Both propellers are with new-foil(Epple) section and operating at σ=0.60 and 10° inclined shaft condition. The design points for P4 propeller and this conventional propeller are almost the same; thus, the efficiencies of these two propellers can be compared with each other. The thrust coefficient, torque coefficient, vertical force coefficient, and efficiency are respectively defined by Equations (4), (5), (6), and (7):

$$K_T = \frac{T}{\rho n^2 D^4} \tag{4}$$

$$K_Q = \frac{Q}{\rho n^2 D^5} \tag{5}$$

$$K_V = \frac{F_v}{\rho n^2 D^4} \tag{6}$$

$$\eta_O = \frac{J}{2\pi}\cdot\frac{K_T}{K_Q} \tag{7}$$

Where T=the propeller thrust, Q=the propeller torque, F_v=vertical force induced by inclined shaft angle, ρ =density of the fluid, n the shaft rotating speed, and D the propeller diameter. However, it is noticed that the propeller thrust T is not thrust along the shaft, but corrected to the direction of the advance speed V_1.

Figure 19 shows the efficiency of the P4 propeller (ENDP) is higher than that of the conventional propeller by 2.2 percent point at the design point (i.e., from 0.659 to 0.681). Because the thrust of the ENDP propeller is mainly contributed by the propeller pressure side, the cavitation on the back of the propeller can be controlled well, and a lower Ae/Ao is allowable. According to this feature of the ENDP propeller, the improvement of the efficiency is due to the possibility of reducing the blade area for the same cavitation behavior and not because the ENDP is more efficient when compared to a propeller with the same main dimensions.

Besides, Figure 20 illustrates the efficiencies of P4 propeller and P5 propeller at different propeller loadings. It shows that the efficiency of the ENDP propeller does not decrease as the propeller loading, K_T/J^2, is increased. The ENDP propeller can also delay the occurrence of thrust breakdown due to the feature mentioned above. Furthermore, the ENDP propeller is more suitable for accelerating condition, because the thrust of the ENDP propeller will not breakdown easily at the heavy-load condition.

As shown in Figure 21, the expanded area ratio of P4 propeller is lower than that of the conventional propeller, but the cavitation phenomena of P4 propeller are similar to that of P5 propeller when propellers operate at σ=0.60 and 8° inclined shaft condition. It illustrates that the ENDP propeller can control the back cavitation on the propeller blade with lower expanded area ratio.

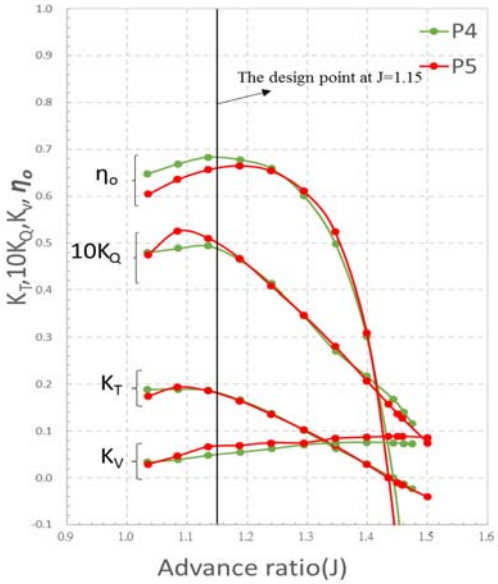

Figure 19. The open-water diagram of the P4 ($Rn_{0.7r} = 1.3\times10^6$) propeller and P5 ($Rn_{0.7r} = 1.9\times10^6$) propeller at σ=0.60 and 10° inclined shaft condition

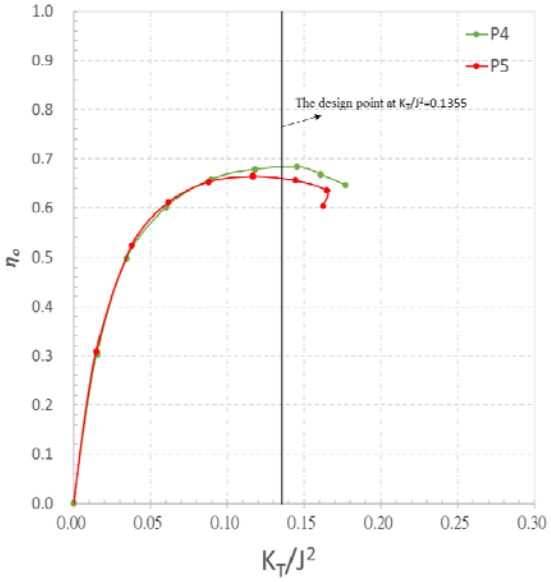

Figure 20. The comparisons of the efficiencies between P4 ($Rn_{0.7r} = 1.3\times10^6$) and P5 ($Rn_{0.7r} = 1.9\times10^6$) at different propeller loadings at σ=0.60 and 10°inclined shaft condition

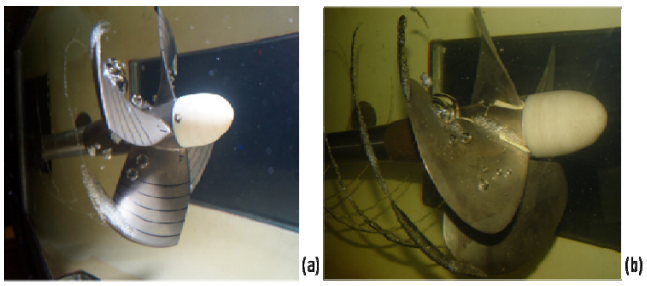

Figure 21 The comparisons of the cavitation between (a) P4, A_e/A_o =0.80 ($Rn_{0.7r}=1.3\times10^6$) and (b) P5, A_e/A_o =1.00 ($Rn_{0.7r}=1.9\times10^6$) at ,J=1.15, σ=0.60 and 8° inclined shaft condition

It is noticed here that bubble cavitation can cause erosion near the trailing edge of the blade, if the cavitation bubbles collapse to cloudy and tiny bubbles before trailing edge. However, if the cavitation bubbles are stable on the trailing edge, the erosion can be avoided. The types of bubble cavitation are depending on the chordwise camber distribution of the propeller.

4 Conclusion

According to the verifications of diffused endplate propeller experiments, the following points can be concluded:

1 The diffused endplate propeller not only can effectively control the propeller tip vortex cavitation but also can eliminate the back sheet cavitation on the outer surface of endplate, often observed for CLT propeller.

2 According to the experimental results, as the propeller operates at zero inclined shaft angle condition, 0.3° diffused angle for the tip endplate of the ENDP propeller is appropriate to eliminate the sheet cavitation on the outer surface of the tip endplate for K_T/J^2 about 0.393. For higher propeller thrust loading a higher diffused angle is needed. It can be determined by CFD.

3 For the inclined shaft condition, the optimal diffused angle for the tip endplate is dependent on many design parameters, especially the shaft inclined angle, cavitation number and propeller thrust loading. Since the propeller thrust loading for high speed craft can not vary too much, it can not be considered as an important parameter for designing the endplate diffused angle. As the inclined shaft angle for high speed craft normally is between 8° to 11° dependent on the ship size and ship speed, 1.0° diffused angle for the tip endplate of the ENDP propeller is suggested for inclined shaft angle higher than 10°. However, if the diffused angle of the endplate is higher than 1.0°, some drawbacks can be observed (i.e. the face cavitation on the inner surface of endplate) when the blade rotates to six-o'clock position. If the inclined shaft angle is lower than 10° and the cavitation number is higher than 0.75, a 0.8° diffused angle for the endplate of the ENDP propeller can be considered.

4 Because the thrust of the ENDP propeller contributed from the pressure side is much more than that of the conventional propeller, the back sheet cavitation of blade can be decreased. Consequently, even using a small expanded area ratio the ENDP propeller can still delay the inception of the thrust breakdown as compared with the conventional propeller, and still keep better efficiency at low cavitation numbers.

References

Bertetta, D, Brizzolara, S, Canepa, E, Gaggero, S, Viviani, M (2012) 'EFD and CFD Characterization of a CLT Propeller'. Hindawi Publishing Corporation International Journal of Rotating Machinery Volume 2012, Article ID 348939, 22 pages

Gómez, GP (1976) 'Una Innovación en el Proyecto de Hélices'. Ingeniería Naval.

Gómez, GP, González-Adalid, J (1992) 'Tip Loaded Propellers (CLT) - Justification of their Advantages over Conventional Propellers Using the New Momentum Theory'. SNAME 50th Anniversary, (1942-1992).

Gómez, GP, González-Adalid, J (1998)'Detailed Design of Ship Propellers'. Book edited by FEIN (Fondo Editorial de Ingenieria Naval), Madrid 1998.

Gaggero, S, Gonzalez-Adalid, J, Perez-Sobrino, M (2016) 'Design of Contracted And Tip Loaded Propellers by Using Boundary Element Methods And Optimization Algorithms'. Applied Ocean Research ,55, 102–129.

Kehr, YZ, Wu, LH (2010) 'Study of efficiency and cavitation characteristics of CLT propeller for high-speed craft'. System Engineering and Naval Architecture, National Taiwan Ocean University, R.O.C.

Sánchez-Caja, A, Sipilä, TP, and Pylkkänen, JV (2006) 'Simulation of the Incompressible Viscous Flow Around an Endplate Propeller Using a RANSE Solver'. 26th Symposium on Naval Hydrodynamics Rome, Italy, 17-22.

Sánchez-Caja, A, González-Adalid, J, Pérez-Sobrino, M, Saisto, I (2012) 'Study of End-Plate Shape Variations for Tip Loaded Propellers Using a RANSE Solver'. 29th Symposium on Naval Hydrodynamics Gothenburg, Sweden, 26-31.